J. Condensed Matter Nucl. Sci. 4 (2011) 56–68

Research Article

Heat Evolution from Pd Nano-powders Exposed to High-pressure Hydrogen Isotopes and Associated Radiation Measurements

Akira Kitamura *, Yu Sasaki, Yuki Miyoshi and Akira Taniike

Division of Marine Engineering, Graduate School of Maritime Sciences, Kobe University, Higashinadaku, Kobe 658-0022, Japan

Akito Takahashi, Reiko Seto and Yushi Fujita

Technova Inc., Uchisaiwaicho 1-1-1, Chiyodaku, Tokyo, Japan

Abstract

Using a twin system for hydrogen absorption, experiments on heat evolution and charged particle generation by D_2 (H_2) gas absorption in nano-sized Pd powders were done for the 0.1 μm. Pd powder, the Pd-black, and the mixed oxides of Pd·Zr, Pd·Ni·Zr and Ni·Zr. It has been found that the D(H)/Pd loading ratio and the absorption energy per D (H) is an increasing function of fineness of the sample surface. The Pd·Zr oxide nano-composites showed anomalously large energies of hydrogen isotope absorption as well as large loading ratio in the phase of deuteride/hydride formation. Although the samples were deteriorated by the repeated baking-hydrogenation cycles, an artificial oxidation of the PZ and the PNZ samples recovered the excellent original performances, and gave hydride formation energies of 1.5–2.3 eV/D and 1.5–2.0 eV/H, which are anomalously high compared with values for bulk Pd metal. In the second phase after the deuteride formation, the Pd·Zr and Pd·Ni·Zr oxide composites charged exclusively with D_2 sometimes gave significantly positive output, which should be subjected to repeated investigation. Nuclear reaction products including energetic charged-particles for a possible cause of the phenomena were examined using a variety of nuclear diagnostics.

Keywords: Anomalous heat, Charged particle measurement, Deuterium absorption, D/Pd loading ratio, Forced oxidation, Isotope effect, Pd·Zr nano-powder, Recovery of performance

PACS: 89.20.-a

1. Introduction

Arata and Zhang recently reported that highly pure D_2 gas charging of Pd nanopowders in the form of Pd/ZrO_2 nano-composite induced significantly higher temperatures inside the reactor vessel than at the outside wall continuing for more than 50 h, while runs with H_2 gas showed almost no temperature difference [1]. To verify that the excess heat

*E-mail: kitamura@maritime.kobe-u.ac.jp

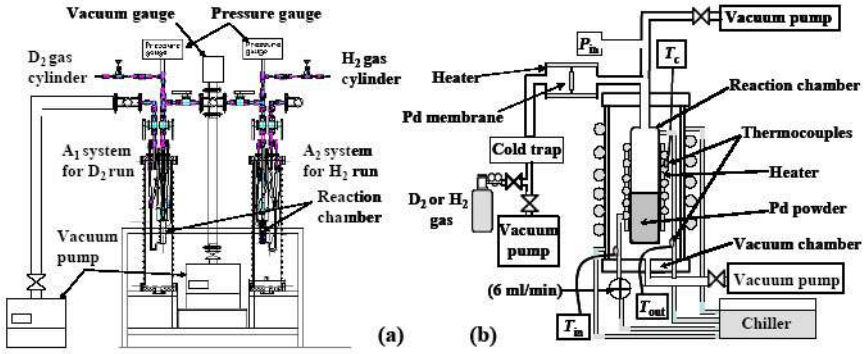

Figure 1. (a) Reduced view of the $A_1 \cdot A_2$ twin system, and (b) functional view of A_1 used in the early stage of the present research. The Pd membrane filter for flow rate control is replaced by a mechanical needle valve, 'Super Needle'.

originated in a nuclear process, a quadrupole mass spectrometer was employed to show the existence of ^{4}He as nuclear ash in the vessel and in the powder after the charging. The charging system is a sophisticated, yet simplified, version of the previous-generation DS reactor [2]. Successful replications using systems similar to the DS reactor with Pd-black have been reported [3,4].

However, few reports on the replication experiments producing heat and ^{4}He with the new configuration have published yet in spite of extreme importance of the phenomenon. It is crucial to confirm the phenomenon of heat and ^{4}He generation with fully quantitative reliability.

We have constructed an experimental system to replicate the phenomenon and to investigate the underlying physics. The system is composed of two identical reaction chambers, an $A_1 \cdot A_2$ twin system, equipped with calorimetry setups, and a B-system for nuclear diagnostics. We report here the results of heat measurements as well as charged particle measurements under deuterium/hydrogen absorption by a variety of Pd nano-powders, covering our former results [11–13] and newer results.

2. Experimental Apparatus for Calorimetry

The D_2/H_2 absorption system is composed of two identical chambers (an $A_1 \cdot A_2$ twin system): one for a D_2 gas foreground run, and the other for H_2 gas background run. As shown in Fig. 1, each part has an inner reaction chamber containing Pd powder and an outer chamber that is evacuated to provide thermal insulation for calorimetry. A sheath heater and a cooling water pipe made of copper are wound on the outer surface of the reaction chamber for baking the sample powder and for flow calorimetry to estimate the heat production rate, respectively. A pair of thermocouples is provided for the flow calorimetry by measuring the temperature difference between the inlet and the outlet of the cooling water.

The D_2 gas is nominally 99.5% pure and the H_2 is 99.998% pure. In the early stage of the present research, flow rate control of D_2/H_2 gas purified through a liquid-nitrogen cold trap was made with a Pd membrane filter which also serves as an additional purifier. The Pd membrane (0.2 mm-t, 99.95%) separates the evacuated reaction chamber (50 cm^3) and the gas reservoir filled with D_2/H_2 at 1 MPa. The gas permeation rate is controllable between 0.1 and 25 sccm by varying the membrane temperature from room temperature to 900 K. However, it was replaced in the latter half of the experiments by a mechanical needle valve, 'Super Needle', because the precision of adjustment of the membrane temperature was found to be rather poor.

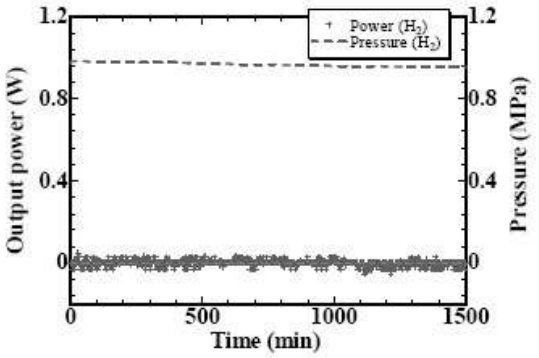

Figure 2. Blank run with no sample powder.

In expectation of occurrence of some nuclear phenomena, a neutron dose rate meter and a scintillation probe for γ-ray detection are located just outside the outer chambers. All parameters measured are stored in a PC with an acquisition period of 1 min.

As a calibration of the flow calorimeter, we measured the heat recovery rate under a variety of conditions; with input power of 1, 3, 6 and 10 W, and D_2 gas pressure of 0, 0.1, 0.3 and 1.0 MPa in the reaction chamber. The coolant flow rate was 6 cm^3/min in all cases. The heat recovery rate was found to be almost independent of the pressure and the input power, and the averaged value is $(63.1 \pm 5.8)\%$. Temperature response to a stepwise variation of the input power was found to be expressed as a simple exponential function with a time constant of 5.2 min.

We examined temperature uncertainty and drift, with no sample powder put in the A_1 chamber filled with H_2 gas at a pressure of 1 MPa. The inlet–outlet temperature difference and the output power deduced from it showed short-term fluctuation as shown in Fig. 2. If we regard an experimental error in the present system as the standard deviation of the longitudinal data, the error or the uncertainty for the output power and the integrated output energy measured for the $A_1 \cdot A_2$ system is evaluated to be 0.014 W and 0.83 kJ for 1000-min acquisition. In the prototype system A_0, which had the larger time constant and smaller sensitivity of heat measurement, and was used in the first stage experiments with the 0.1-μmϕ Pd powder and the Pd-black [5], a temperature drift observed sometimes resulted in the larger error of 4.0 kJ for 1000-min run.

In the following, the run number is designated by "G-PN#M", with G, P, N and M being the gas species, the powder species, powder ID, and the number of repeated use, respectively. The powder species include PP (Pd powder with particle diameter of 0.1 μm and a purity of 99.5%), PB (Pd-black with a particle size of "300 mesh" and purity of 99.9%), PZ (mixed oxides of Pd·Zr), PNZ (mixed oxides of Pd·Ni · Zr) and PN (mixed oxides of Ni·Zr). For example, "D-PB2#3" represents the third absorption run with D_2 using a Pd-black sample "2" following evacuation and baking after two cycles of evacuation-baking-absorption. All D_2/H_2 gas absorption runs described below were conducted at room temperature.

Three kinds of mixed oxide samples, PZ, PNZ and NZ, were fabricated by Santoku Corporation, Kobe, Japan. The physical properties of these samples are tabulated in Table 1. The PZ samples have an average particle size of 7.7–20 μm, a specific surface area of 37–41 m^2/g, and an average Pd grain size of 10.7–8.3 nm. Since X-ray diffraction measurements of the PZ sample have revealed presence of PdO, we have to assume that 10 g of the sample contains 3.0–3.3 g of Pd depending on the degree of oxidation of Pd. In the sample PNZ, substantial part of Pd is replaced by Ni also in the form of NiO with a molar fraction of about 25%, while Pd is completely replaced by Ni with a larger

Table 1. Physical properties of Pd·Ni·Zr oxide samples prepared by Santoku Corp. The fraction depends on the degree of oxidation of Pd, i.e., the ratio of PdO to Pd.

Sample name		PZ		PNZ	NZ
Lot number		081030	090529-1	090609-1	090609-2
Molar fraction	Pd	0.346	0.356	0.105	
	Ni			0.253	0.358
	Zr	0.654	0.644	0.642	0.642
	O	1.31–1.65	1.29–1.64	1.54–1.64	1.64
Weight fraction	Pd	0.314–0.299	0.328–0.308	0.103– 0.101	
	Ni			0.135–0.133	0.197
	Zr	0.508–0.485	0.501–0.478	0.537–0.529	0.555
	O	0.178–0.215	0.176–0.214	0.537–0.237	0.249
Average particle size (mm)		7.7	20.3	23.7	15.5
Specific surface area (m^2/g)		37.1	41.3	35.2	27.6
Average grain size (nm)		10.7	8.3	7.4	(Ni) 23.2

grain size of 23 nm in the sample NZ. In the following analysis of the data for the PZ samples, we use an average value of 0.314 for the weight fraction of Pd, which introduces a systematic error of about 5% to the values of the loading ratio D(H)/Pd and the first phase absorption energy E_{1st} which is considered to be equal to the heat of solution or the hydride formation energy Q_D (Q_H). In the present paper the word "hydride" stands for the deuteride and the hydride in the customary sense.

3. Results of Calorimetry

3.1. 0.1-μmϕ Pd powder (PP)

First of all, we describe absorption runs using the A_0 system for 5 g of commercially available 0.1-μmϕ Pd powder. The reaction chamber filled with the powder was evacuated and heated for baking at 430 K. Then highly pure D_2 or H_2 gas was introduced into the reaction chamber through the Pd membrane filter. The results for the case of D_2 and H_2 absorption are compared in Fig. 3(a). After the gas is introduced, pressure does not begin to rise for a while. During this phase (the first phase) the Pd powder absorbs almost all of the D_2 (H_2) gas atoms as they flow in, and heat is released as a result of adsorption and formation of deuterides (hydrides). After about 30 min, the powder almost stops absorbing gas; the gas pressure begins to rise, and the heat release from deuteride (hydride) formation subsides. This is the beginning of the second phase, and the gas flow rate in the first phase is evaluated from the rate of the pressure increase. From the flow rate multiplied by the duration of the first phase, loading is estimated to reach $PdD_{0.46}$ ($PdH_{0.45}$). The loading ratios, i.e., H(D)/Pd values, might be smaller by about 30% than those evaluated at the final pressure of 1 MPa, since the pressure is still low at this moment. This possible underestimation of the loading ratio would lead to overestimation of the first phase absorption energy E_{1st} calculated as follows by the same amount.

The output power is integrated over the first phase to give the output energies of 0.10 kJ/g-Pd(D) and 0.08 kJ/g-Pd(H), which are divided by the loading ratio of 0.46 and 0.45 to give the first phase absorption energy E_{1st} or the hydride formation energy Q_D of 0.24 eV/atom-D and Q_H of 0.20 eV/atom-H, respectively. The values appear to be somewhat larger than those found in the literature [6–10]. However, they are consistent with each other, when we take into account that the differential heat of solution is a decreasing function of the loading ratio; $Q_H = 0.15$, 0.12, 0.070, and 0.061 eV/H for H/Pd ratio of 0.5, 0.55, 0.6 and 0.65 [9,10]. The difference between D and H, the isotope effect, is rather large, but is not considered to be anomalous, since we find $Q_D/Q_H = 1.25$ in [9]. The difference is even considered to be meaningless in view of the experimental error shown by the values following '±' in the fifth column.

On the other hand, the output energy in the second phase, i.e., the output power integrated over the second phase

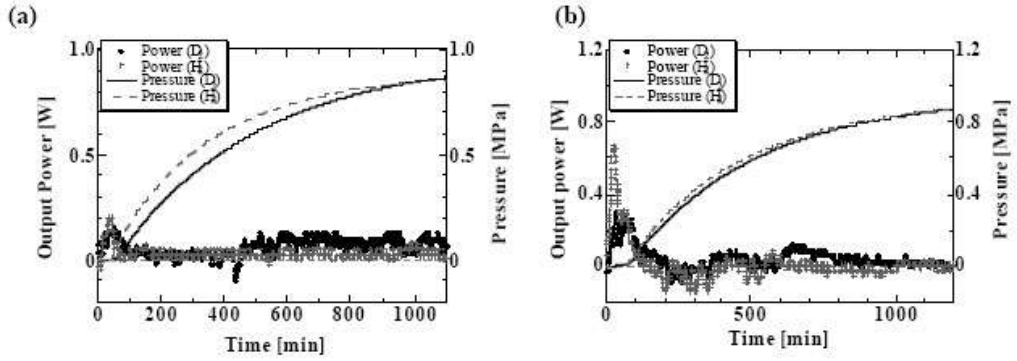

Figure 3. Evolution of heat and pressure in the vessel after pumping D_2 gas or H_2 gas; (a) 0.1-μmϕ Pd powder (D-PP1#1 and H-PP2#1), (b) 300-mesh Pd-black (D-PB1#1 and H-PB2#1).

with duration of 1,400 min, is smaller than the experimental error mentioned above, and is therefore meaningless. The results are summarized in Table 2, which includes those for the Pd-black sample described below.

3.2. 300-Mesh Pd-black (PB)

The second kind of the sample tested is commercially available, 300-mesh Pd-black whose surface has a kind of nano-scale fractal structure finer than the 0.1-μmϕ Pd powder. The performance of the Pd-black absorption of D_2 using the A_0 system is compared with that of H_2 in Fig. 3(b). It is very interesting to note that: (1) much higher loading to $PdD_{0.82}$ or $PdH_{0.78}$ is realized, and (2) the output energies in the first phase, E_{1st} = (0.68.0.12) eV/atom-D and (0.63 .0.11) eV/atom-H, are 2–3 times larger than those for the 0.1-μmϕ Pd powder and those found in the literature [6–10]. On the other hand, the output energy of 8.3±4.5 kJ (2.6±1.4 kJ/g-Pd) in the second phase of D_2 absorption appears to be larger than that in the case of H_2. The difference, however, is only marginal compared with the above-mentioned error due to the temperature drift of 5.5 kJ in the present case.

Using the improved twin system $A_1 \cdot A_2$, we compared the performance of the Pd-black sample PB3 with a prolonged duration of the second phase of 4,500 min, which was subjected to repeated use with the sample baking before absorption at 440 K for 3 h (No. 2), or at 570 K for 1 h (No. 3). The results are shown in the sixth row through the eighth in Table 2.

Table 2. Comparison of absorption runs for the 0.1-μmϕ Pd powder (PP), and the 300-mesh Pd-black (PB).

Run	Weight (g)	Pd weight (g)	First phase				Second phase
			Flow rate (sccm)	Specific output energy E_1 (kJ/g-Pd)	D/Pd or H/Pd	E_{1st} per D or H atom (Q_D or Q_H) (eV)	Specific output energy E_2 (kJ/g-Pd)
D-PP1#1	5	5	3.5	0.10±0.07	0.46	0.24	0.52±0.83
D-PP1#2	5	5	4.3	0.10±0.05	0.43	0.26	0.79±0.88
H-PP2#1	5	5	6.8	0.08±0.003	0.45	0.20	0.53±0.8
D-PB1#1	3.2	3.2	3.5	0.54±0.10	0.85	0.70	2.6±1.4
H-PB2#1	3.6	3.6	5.6	0.45±0.08	0.78	0.63	-0.62 ± 1.3
D-PB3#1	20	20	2.9	0.47±0.06	0.78	0.66	0.06±0.02
D-PB3#2	20	20	0.8	0.17±0.03	0.23	0.82	0.17±0.13
H-PB4#2	20	20	1.9	0.16±0.01	0.22	0.80	0.68±0.23

First we notice that the first run (D-PB3#1) has essentially the same D/Pd ratio and the output energy E_{1st} as that for the A_0 system. Second, the repeated use retains almost the same or even higher output energy E_{1st} in spite of the significantly smaller D(H)/Pd ratio. This interesting fact could be related to some structural change of the sample. The SEM photograph of the sample indicates an image of clumping-together of the sample flakes and disappearance of the fine structure on the scale of several tens of nm. This point will be discussed in detail later elsewhere. As for the second phase, we have little to discuss, when we take into account that they are comparable to the error of 4.0 kJ/1000-min mentioned above for the A_0 system.

3.3. Mixed oxides of Pd·Zr (PZ)

Now we describe the performance of the mixed oxides of Pd·Zr that are thought to have an even finer mesoscopic structure. The results of fourteen runs using PZ samples are summarized in Table 3. These include runs with virgin PZ samples (No. 1) and used PZ samples (Nos. 2 and 3). Using the A1·A2 twin system, the runs H-PZ(2n) No. 1 were performed simultaneously with D-PZ($2n-1$) No. 1, where $n = 1, 2, 3$ and 5. The A_1 subsystem was used for D-PZ1, D-PZ3, D-PZ9 and H-PZ6, and the A2 subsystem for H-PZ2, H-PZ4, H-PZ10 and D-PZ5. Note that the subsystem was permutated for D-PZ5 and H-PZ6 intentionally to confirm that which reaction chamber to choose does not matter. The PZ sample used was 10 g or 14 g, and the baking temperature was 570 K for 3 h. The output energy in the second phase is the power integrated over 1,600 min. Examples of the evolution of the output power and the pressure for runs D-PZ1#1 and H-PZ2#1 are shown in Fig. 4.

To deduce the values of D/Pd (H/Pd), we have assumed that the pressure change is caused solely by consumption of D_2 (H_2) gas due to the formation of PdD (PdH). As mentioned earlier, some fractions of Pd atoms in the Pd.Zr oxide samples may be in the form of PdO. X-ray diffraction measurements after D (H) absorption experiments have revealed almost perfect reduction to Pd to replace D_2 (H_2) by D_2O (H_2O) molecules. If the D_2O (H_2O) molecules happen to condense into the liquid phase to give almost no contribution to the gas pressure, the reduction of PdO could lead to overestimation of the amount of the D_2 (H_2) gas absorbed by Pd, and therefore of the values of D/Pd (H/Pd). However, the sample is in vacuum, and therefore the water molecules will remain in the gas phase at least until we evaluate the

Table 3. Comparison of absorption runs for the Pd.Zr nano-composite (PZ).

Run	Weight (g)	Pd weight (g)	First phase			Second phase	
			Flow rate (sccm)	Specific output energy E_1 (kJ/g-Pd)	D/Pd or H/Pd	E_{1st} per D or H atom (eV)	Specific output energy E_2 (kJ/g-Pd)
D-PZ1#1	10	3.14	1.76	2.30±0.06	1.03	2.47	2.09±0.90
H-PZ2#1	10	3.14	2.29	1.17±0.04	0.95	1.35	-1.69 ± 0.91
D-PZ3#1	10	3.14	1.85	2.10±0.06	1.03	2.26	2.11±0.80
H-PZ4#1	10	3.14	2.93	1.63±0.03	0.82	2.19	−0.11±0.80
D-PZ3#2	10	3.14	1.66	0.05±0.01	0.28	0.20	2.49±0.67
H-PZ4#2	10	3.14	2.79	0.20±0.02	0.29	0.77	0.62±0.67
D-PZ3#3	10	3.14	1.69	0.10±0.02	0.24	0.48	0.21±0.40
H-PZ4#3	10	3.14	2.99	0.17±0.01	0.25	0.73	0.11±0.40
D-PZ5#1	10	3.14	2.02	2.28±0.05	1.00	2.52	0.40±0.48
H-PZ6#1	10	3.14	6.23	2.34±0.03	1.35	1.91	-0.08 ± 0.48
D-PZ5#3	10	3.14	9.93	0.16±0.01	0.24	0.74	-0.50 ± 0.48
H-PZ6#3	10	3.14	10.69	0.27±0.01	0.29	1.02	−0.07±0.48
D-PZ9#1	14	4.41	6.42	2.33±0.02	1.34	1.92	0.87±0.34
H-PZ10#1	14	4.41	20.49	2.18±0.01	0.97	2.48	0.87±0.34
D-PZ#1 avrg	—	—	—	2.25±0.10	1.10±0.16	2.29±0.27	1.37±0.87
H-PZ#1 avrg	—	—	—	1.83±0.53	1.03±0.23	1.98±0.48	-0.25 ± 1.06

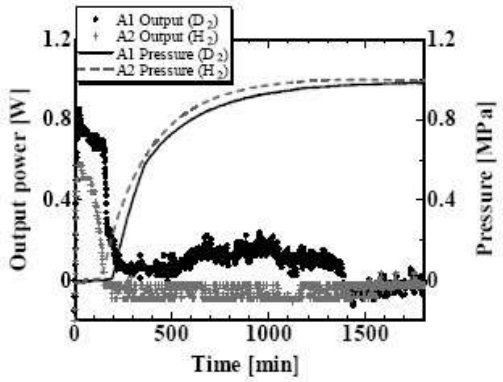

Figure 4. Evolution of heat and pressure in the vessel after pumping D_2 gas or H_2 gas for mixed oxides of Pd and Zr (D-PZ1#1 and H-PZ2#1).

rate of pressure increase, which, multiplied by the duration of the first phase, is used to calculate the amount of D_2 (H_2) gas absorbed into the sample. Therefore, there is little chance to overestimate the amount of the gas absorbed for the formation of PdD(H), since the same volume of D_2O (H_2O) is liberated in the gas phase in exchange for consumption of D_2 (H_2) for the PdO reduction.

To evaluate the values of Q_D or Q_H, we have to know the extent to which the Pd atoms are oxidized. For this purpose, assuming that a fraction x of the Pd atoms are oxidized, we examine reduction of PdO_x followed by production of xD_2O (xH_2O) and PdD_y (PdH_y). The total reaction energies are evaluated to be $(1.69x + Q_D y)$ eV/atom-Pd and $(1.63x + Q_H y)$ eV/atom-Pd, respectively. The values of Q_D and Q_H for the bulk Pd cited from the references [6–10] lie in the range from 0.2 to 0.7 eV. Since we do not know the values of x for the given samples, we leave E_{1st} in the seventh column in Table 3, and do not dare to obtain the values of Q_D and Q_H from the measured quantities for the moment. This point will be discussed later in this subsection.

We notice in Table 3 the following three facts in the first phase of the No. 1 runs, i.e., for virgin samples: (1) very large D/Pd (H/Pd) ratio of about 1.1±0.2 (1.0±0.2) that are even higher than those for the PB samples, (2) surprisingly large E_{1st} = (2.3.0.3) eV (D) and (2.0±0.5) eV (H) on average, and (3) a modest isotope effect in E_{1st} consistent with those for 0.1-μmϕ powder and Pd-black; the difference does not exceed the error range determined from the standard deviations in contrast to our former report [11–13] which does not include the runs D(H)-PZ9(10) No. 1.

On the other hand, for used samples, i.e., in the runs with the run numbers 2 and 3, we observe smaller D/Pd (H/Pd) ratios which are essentially the same as those for the used PB samples mentioned in the preceding subsection, and E_{1st} values similar to those for PB and PP samples with a few exceptions. It is inferred that these are due to the clumpimg-together effect mentioned above for the PB samples. TEM photographs of the samples taken by the courtesy of the Nuclear Science and Engineering Institute and Particulate Systems Research Center at the University of Missouri-Colombia showed that the Pd nano-particles are bunched together to form clusters consisting of tens to hundreds of Pd nano-particles. The absorption–desorption or heating-cooling history of the sample might have a crucial effect on the hydrogen absorption characteristics.

We have anomalously large absorption energies and loading ratios in the present mesoscopic system of virgin Pd.Zr oxides. It should be mentioned here that we cannot assume large contribution of ZrO_2 to these quantities. This is because the NZ samples fabricated in the same way as the PZ samples absorb essentially no D_2 (H_2) gas, and there is no output energy, as described in the next subsection.

Next, to examine the contribution of PdO reduction to E_{1st}, the used PZ1 and PZ2 samples were artificially oxidized

Table 4. Artificial oxidation to find the D(H) absorption energy for the Pd.Zr nano-composite (PZ). It is assumed that the reaction proceeds via oxygen pickup from PdO_x followed by hydridation to PdD_y (PdH_y), i.e. $PdO_x + (x + y/2)D_2 \rightarrow xD_2O+PdD_y$, the absorption energy Q_D (Q_H) is calculated from the relationship; $E_{1st}.y = Q_{red}.x + Q_{D(H)}.y$ (eV/Pd), where the reduction energy $Q_{red} = 1.69$ (1.63) eV for D (H) is assumed: (m), (c) and (a) mean "measured", "calculated" and "assumed", respectively.

Run	First phase						Second phase	Remarks
	Flow rate (sccm)	Specific output energy E_1 (kJ/g-Pd)	D/Pd or H/Pd ($= y$)	E_{1st} per D/H atom (eV)	O/Pd ($= x$)	Q_D or Q_H (eV/D(H))	Specific output energy E_2 (kJ/g-Pd)	
D-PZ1#3	7.88	1.45±0.01	0.97 (m)	1.73 (m)	0.081 (m)	1.59 (c)	1.37±1.28	Artificially
H-PZ2#3	12.12	0.89±0.01	0.65 (m)	1.57 (m)	0.048 (m)	1.45 (c)	0.29±1.28	oxidized
D-PZ*#1 avrg	—	2.25±0.10	1.10 (m)	2.29 (m)	0.459 (c)	1.59 (a)	1.08±0.67	Q_D and Q_H
H-PZ*#1 avrg	—	1.83±0.53	1.03 (m)	1.98 (m)	0.334 (c)	1.45 (a)	−0.63 ± 1.34	assumed.

by keeping them in O_2 atmosphere. The sample vessel was initially filled with O_2 gas at a pressure of 0.1 MPa, and kept at a temperature of 470 K for 33 h without supplying additional O_2 gas into the closed vessel. Assuming that the samples had no oxygen before this process, the extent of the sample oxidation, i.e., x for PdO_x, was calculated from the pressure drop in the reaction vessel. The values of x were rather modest, below 10%, which are given in the sixth column in Table 4.

The D_2 (H_2) absorption runs after the oxidation, D-PZ1#3 and H-PZ2#3, showed substantial recovery of D(H)/Pd and E_{1st}, as shown in the upper two rows in Table 4. Since we know the values of x for these samples, we can eliminate the reduction energy from E_{1st} to obtain the hydride formation energy, Q_D (Q_H). It is assumed here that the reaction proceeds via oxygen pickup from PdO_x followed by hydridation to PdD_y or PdH_y; $PdO_x + (x + y/2)D_2 \rightarrow xD_2O+PdD_y$, or $PdO_x + (x + y/2)H_2 \rightarrow xH_2O+PdH_y$. The hydride formation energy Q_D (Q_H) is calculated from a relationship; $E_{1st}y = Q_{red}\,x + Q_{D(H)}\,y$ (eV/Pd), where the reduction energy $Q_{red} = 1.69$ (1.63) eV for D(H) is assumed. In the table, (m), (c) and (a) stand for "measured", "calculated" and "assumed", respectively. It is found that the hydride formation energies, $Q_D = 1.59$ eV and $Q_H = 1.45$ eV, are about twice as large as those for the PB samples, and about 6∼7 times larger than for the PP samples or the published values for the bulk Pd.

Once we know Q_D (Q_H), we can estimate x for the PZ samples using the same relationship, under the assumption that the hydride formation energies Q_D and Q_H remain unchanged after the oxidation process. These are shown in the lower two rows in Table 4. We see that rather reasonable values of x =0.46–0.33 are obtained.

Finally, we examine the second-phase heat evolution. We have negative values for the specific output energy E_2 in some runs mainly using H_2, as seen in Tables 2 and 3. This should be considered to be due to a possible baseline shift of the thermocouple signal. In contrast to the runs with H_2, positive output signals exceeding the error range have been observed in several runs with D_2, as typically shown in Fig. 4. This implies that some nuclear process could be involved, although the values are only marginal in view of the negative value observed in H-PZ2#1. These points should be subjected to further investigation.

3.4. Mixed oxides of Pd·Ni·Zr (PNZ) and Ni·Zr (NZ)

Next, the performances of the mixed oxide samples PNZ and NZ are described. The former type of the mixture was used in [1], and was found, they say, to give the best performance for the "excess" heat generation. The results of eight runs using the PNZ samples are summarized in the upper eight rows in Table 5. Similar to the runs using the PZ samples, the runs H-PNZ2#m were performed simultaneously with D-PNZ1#m, where $m = 1, 2, 3$ and 4. The samples PNZ1 and PNZ2 remained in each reaction chamber during these runs. Table 5 also includes the results of two runs using the NZ samples in the last two rows. The PNZ or NZ samples used were 10 g or 20 g, each containing 1.02 g or 0 g of Pd, respectively. The processing conditions for baking and oxidation were similar to those for the PZ samples.

We see that the loading ratio, D(H)/Pd, and the output energy in the first phase, E1st, evaluated for one D(H) atom are essentially the same as those for the PZ sample. Also similar to the PZ sample is the much smaller D(H)/Pd ratio in the No. 2 runs. At the first glance, these facts mean that Ni has no contribution to the heat evolution. However, some features similar to those for the PNZ sample are observed. One is that E_{1st} does not significantly decrease in the No. 2 runs.

The other is the effect of artificial oxidation of the sample. The oxidation provides a distinguished recovery of the high values of E1st and a modest recovery of the D(H)/Pd ratios, as can be seen in the Nos. 5–8 runs with artificial oxidation of the used samples. Similar to the PZ sample, the modest oxidation of 3–6% has induced a modest recovery of D(H)/Pd and a pronounced recovery of E_{1st} to the initial values. As has been done for the PZ sample, Q_D (Q_H) is calculated from the known values of x to find even higher values than for the PZ sample. Again, we apply the mean values of Q_D (Q_H) to estimate x for the virgin samples to confirm reasonable values of x. The same procedure is applied to the reused samples supplied for the No. 2 runs. The values of x are negative but nearly equal to zero, which implies that the above procedure is quite reasonable.

Concerning the NZ sample, we have observed definitely no interval with $p = 0$ nor any positive outlet–inlet temperature difference; the NZ sample gives negligibly small D(H) absorption rate and heat evolution. This fact confirms that not only Ni in the present samples has only a second-order effect on the hydrogen absorption and heat evolution but also that the ZrO_2 matrix has no effect on the hydrogen absorption nor heat evolution. We confirm also that the sample NZ has negligible amount of impurity elements except oxygen. The same is true also for the PZ and the PNZ samples, since these samples were fabricated using the same recipe. These points assure validity of the statements made for the PZ and the PNZ samples in the preceding subsections.

For the PNZ sample we have observed a positive output signal in the second phase exceeding the error range recorded for more than two days. We have to look into a possible zero-level drift of the thermocouple signal, before concluding a positive output power in the second phase.

3.5. Summary of heat measurements

We claim in the present work that;

(1) The absorption energy E_{1st} increases in function of the fineness of the sample surface, and these samples are ranging from the 0.1-μmϕ Pd powder (PP), the 300-mesh Pd-black (PB) and the oxide composites of Pd·Zr

Table 5. Results of runs using samples containing Ni, PNZ and NZ. The same procedure was applied to obtain Q_D and Q_H for Nos. and runs, and to estimate x for Nos. 1 and 2 runs.

Run	First phase						Second phase	Remarks
	Flow rate (sccm)	Specific output energy E_1 (kJ/g-Pd)	D/Pd or H/Pd ($= y$)	E_{1st} per D/H atom (eV)	O/Pd ($= x$)	Q_D or Q_H (eV/D(H))	Specific output energy E_2 (kJ/g-Pd)	
D-PNZ1#1	5.57	1.74±0.03	0.94 (m)	2.05 (m)	0.156 (c)	1.77 (a)	1.01±0.45	$Q_D(Q_H)$ assumed to calculate x
H-PNZ2#1	11.12	1.86±0.03	0.94 (m)	2.19 (m)	0.262 (c)	1.73 (a)	0.10±0.45	
D-PNZ1#2	5.37	0.12±0.03	0.10 (m)	1.28 (m)	−0.029 (c)	1.77 (a)	5.78±3.18	
H-PNZ2#2	11.37	0.14±0.03	0.11 (m)	1.44 (m)	−0.019 (c)	1.73 (a)	2.18±3.18	
D-PNZ1#3	5.21	0.73±0.02	0.39 (m)	2.09 (m)	0.044 (m)	1.89 (c)	0.91±0.72	Artificially oxidized
H-PNZ2#3	11.14	0.75±0.02	0.41 (m)	2.01 (m)	0.032 (m)	1.89 (c)	−0.66 ± 0.72	
D-PNZ1#4	5.43	0.84±0.03	0.50 (m)	1.85 (m)	0.063 (m)	1.64 (c)	−0.31±1.83	
H-PNZ2#4	12.01	0.87±0.02	0.56 (m)	1.72 (m)	0.047 (m)	1.58 (c)	−0.03±1.85	
D-NZ1#2	7.01	0.0 (Ni)	0.0 (/Ni)	—	—	—	0.0 (/Ni)	
H-NZ2#2	13.05	0.0 (Ni)	0.0 (/Ni)	—	—	—	0.0 (/Ni)	

(PZ) or Pd·Ni·Zr (PNZ).

(2) For the PB sample, the loading ratios D/Pd = 0.82 or H/Pd = 0.78 and the output energies in the first phase, E_{1st} = (0.68 ± 0.12) eV/atom-D or (0.63±0.11) eV/atom-H, were both 2–3 times larger than those for the 0.1-μmϕ. Pd powder and those found in the literature.

(3) The PZ sample shows an outstanding performance concerning the high loading ratios D/Pd = 1.1 ± 0.2 and H/Pd = 1.0 ± 0.2, as well as the high absorption energies E_{1st}, or the deuteride (hydride) formation energy Q_D and Q_H ranging from 1.5 to 2.3 eV/D and from 1.5 to 2.0 eV/H depending on how much fraction of the PdO_x reduction energy is included in the measured values of E_{1st}.

(4) The outstanding performance of the PZ sample, which deteriorates because of its repeated use and/or the baking treatment, is shown to be restored significantly by oxidizing a small amount (only less than 10%) of the sample.

(5) The PNZ sample exhibits a performance similar to that shown for the PZ sample, when evaluated from the values per one Pd atom. It shows an even more pronounced recovery after the oxidizing process.

(6) The NZ sample absorbs no hydrogen isotopes.

(7) As for the second phase, we have positive output exceeding the error range for the deuterium runs employing both the virgin PZ and the used PZ samples and the PNZ sample, which should be confirmed by further investigation.

4. Search for Reaction Products

4.1. Neutron and gamma-ray measurement and residual activity

Among possible nuclear reaction products, neutrons and γ rays could be detectable outside the gas absorption chamber. During the absorption runs using the A_1·A_2 system, these were simultaneously monitored with a BF_3 neutron dose rate meter and a scintillation probe for γ ray detection, respectively, with a solid angle of about 0.2 and 0.1 sr [11–13]. Radio activity of some samples after the absorption runs was also measured with use of an imaging plate. However, we have not succeeded in finding meaningful signals in these measurements.

4.2. System B for charged particle measurement

To detect energetic charged particles is the most convincing method to demonstrate the existence of the nuclear phenomenon. The charged particles have a mean free path or a range too small to allow measurements outside the chamber wall. An experimental system shown schematically in Fig. 5 was prepared for charged particle measurements independent on the $A_1 \cdot A_2$ heat measurement system. A solid state detector, a Si surface barrier detector (SSBD) or an ion implanted Si detector (IISD), is located inside the reaction chamber containing a sample holder on which tens of milligrams of the Pd.Zr oxide complex samples are mounted. A sheath heater is wound around the holder for sample baking, and the holder temperature is measured with an alumel–chromel thermocouple attached to the side of the holder. During the sample baking a retractable thermal-shield plate is inserted between the sample and the SSBD/IISD to avoid its deterioration by heating. Energy calibration of the SSBD/IISD is done with the use of an ^{241}Am checking source placed on the retractable shield. During the calibration and before deuterium absorption runs, the chamber is evacuated by a TMP-diaphragm pumping kit. The deuterium gas is introduced into the reaction chamber through a liquid nitrogen cold trap and a "Super needle" valve which enables precise control of the gas flow rate.

4.3. Examples of the Measurement

In the initial stage of this study, we used an SSBD with a depletion layer thickness of 200 μm and the used sample PZ1. The energy spectra recorded during a 5-day run DPZ1# 3B through D-PZ1#4B and evolution of the counting are shown in Fig. 6(a) and (b), respectively.

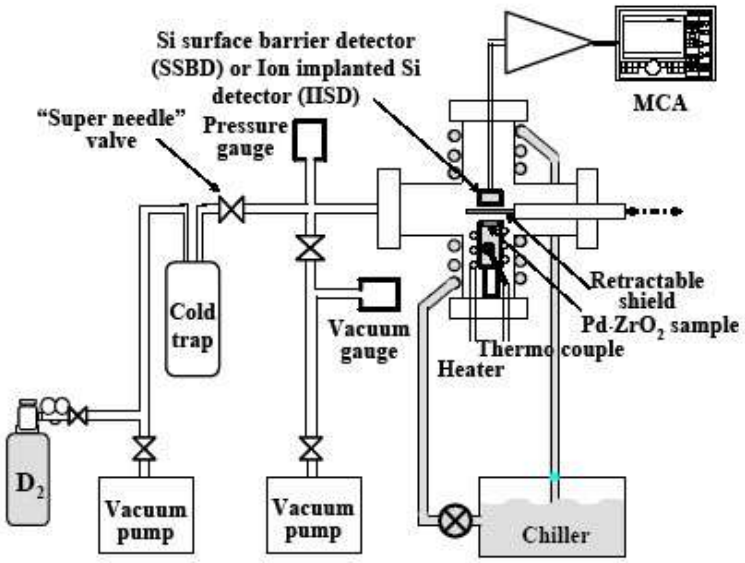

Figure 5. Schematic of the system B for particle measurement.

We see several counts within the energy range from 2 to 4 MeV and a few counts from 7 to 9 MeV. Although these counts could be due to charged particles, we cannot rule out the possibility that this might be caused by electronic noise induced by mechanical shock or oscillation. It is shown in Fig. 6(b) that these counts increase during the period of time at which the pressure changes. Although it is fascinating to imagine that some nuclear events may occur when deuterium atoms flow into/out of the Pd lattice, we cannot conclude it at present.

It is known that any SSBD suffers from deterioration or breakdown when it is used in hydrogen atmosphere. The output pulse height from the SSBD used in the run D-PZ1#3B through D-PZ1#4B was reduced by a factor of about

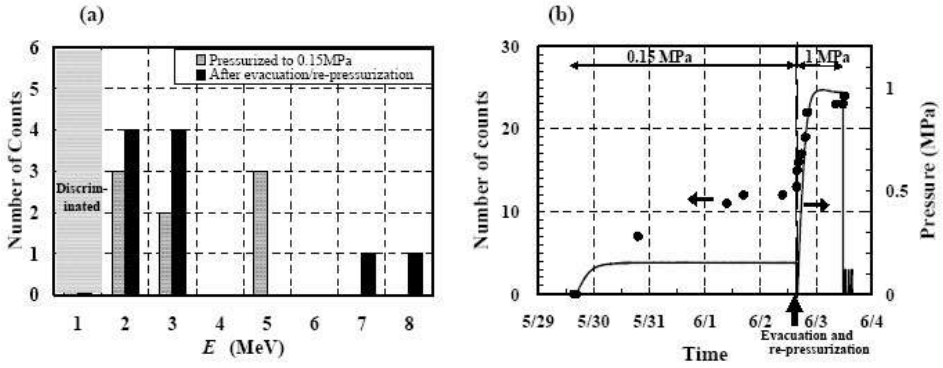

Figure 6. (a) Spectra recorded by SSBD with a 200-μm-thick depletion layer and (b) Evolution of counting in the "1–12 MeV" range of the spectra measured by the SSBD during the run DPZ1# 3B through D-PZ1#4B.

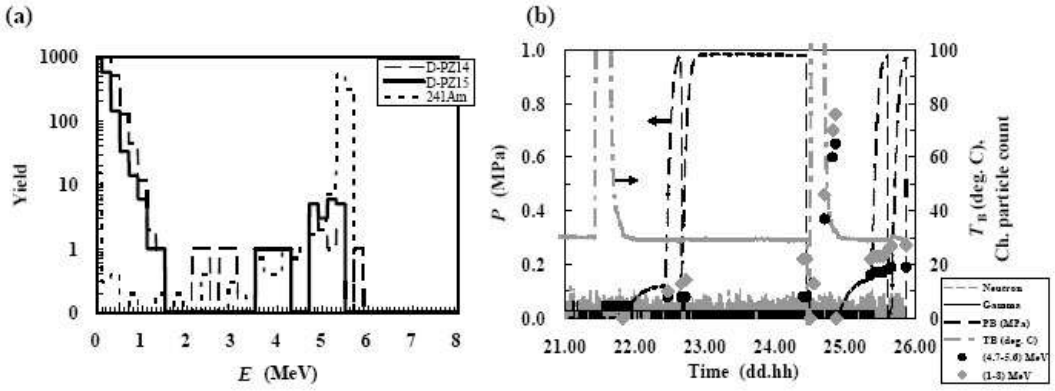

Figure 7. (a) Spectra recorded by the IISD with a 500-μm-thick depletion layer and (b) Evolution of pressure and IISD counting and other radiations during the runs D-PZ14#1B through D-PZ15#2B.

30% and the FWHM increased by a factor of about 5. Although the deteriorated characteristics was stabilized after the initial use for several hundred hours, it was better to abandon it in succeeding runs using virgin samples. We used an IISD with a depletion layer thickness of 500 μm which is known to endure use in hydrogen atmosphere.

Figure 7(a) and (b) show the energy spectra and evolution of pressure and counting of the IISD and other radiations monitored outside the reaction chamber during the runs of D-PZ14#1B, D-PZ15#1B and D-PZ15#2B. The broken line in (a) shows the spectrum of ^{241}Am-α particles used for energy calibration of the detectors. We observe several tens of counts within the energy range of 2–5 MeV during these runs. In (b) the IISD countings are integrated over the runs D-PZ14#1B, D-PZ15#1B-2B, and the baking period. They are reset between the operations.

The integrated IISD counting increased during the baking period between D-PZ14#1B and D-PZ15#1B, which is largely occupied (85%) by the signals lying in the energy range of 4.7–5.6 MeV. This indicates that the upper surface of the retractable shield plate is contaminated by ^{241}Am. From the active surface of the IISD we could see the contamination spot in case of insufficient retraction of the shield plate during the runs. This can account for the increase of the counting also during the runs D-PZ14#1B and DPZ15# 1B-2B.

As shown in Fig. 7(a), the spectra during these runs are a little different from that of the ^{241}Am-α particles, which is also indicated by the difference between the counting in the energy range of 1–8 MeV and that in the range of 4.7–5.6 MeV. The energy shift of the ^{241}Am-α particles by about 0.8 MeV is consistent with the energy loss of 5.486 MeV α-particles in a 5 mm.MPa hydrogen gas. We see again, however, a tendency that the counting increases during the phase of pressure change. It could be possible that the signals lying in the energy range of 2.0–4.5 MeV originate in charged particles emitted by nuclear effects in the sample.

4.4. Summary of charged particle measurements in gas charging system

We have observed several tens of counts within the 1–10 MeV range, which appeared to be emitted coincidentally with pressure change. However, we cannot rule out the possibility that they are due to electronic noise or contamination of ^{241}Am. Up to now, we have no firm evidence of charged particle emission, nor burst of high energy particles corresponding quantitatively to any heat observed in the $A_1 \cdot A_2$ twin system. There remains a possibility that the conditions including the gas pumping were not suitable for the possible excess heat evolution. We are planning to detect X-rays as another candidate to evidence the reaction products.

5. Concluding Remarks

Using the twin system, characteristics of deuterium/hydrogen absorption and accompanying heat generation have been compared for different types of Pd powders; the 0.1-μmϕ Pd powder, the Pd-black, and the mixed oxides of Pd·Zr, Pd·Ni·Zr and Ni·Zr. It has been found that the D(H)/Pd ratio and the absorption energy increase in function of fineness of the sample surface.

The Pd.Zr oxide nano-composites showed anomalously large energies of hydrogen isotope absorption exceeding 2.0 eV as well as large loading ratio exceeding 1.0 in the phase of deuteride/hydride formation. Although the samples were deteriorated by the repeated baking-hydrogenation cycle, an artificial oxidation of the PZ and the PNZ samples recovered the excellent performance of these samples, giving the hydride formation energy of 1.5–2.3 eV/D and 1.5–2.0 eV/H depending on how much fraction of the PdO_x reduction energy is included in the measured values of E_{1st}.

In the second phase after the deuteride formation, the Pd.Zr and Pd.Ni.Zr oxide composites charged exclusively with D_2 sometimes gave significantly positive output, which requires further investigation.

There might be a yet-unknown atomic/electronic process governing the first-phase phenomenon in the present mesoscopic system, or the concept of "atom clusters" [14] might be applied. However, it seems rather difficult to assume that such a large isotope effect observed especially in the second-phase is only due to electron transfer within the process of adsorption and/or hydride formation. Nuclear effects could be one of the candidates responsible for this phenomenon. The 4D-TSC fusion model [15, 16] is one of the most probable scenarios.

References

[1] Y. Arata, Y. Zhang, The special report on research project for creation of new energy, *J. High Temp. Soc.* (1) (2008).
[2] Y. Arata, Y. Zhang, *Condensed Matter Nuclear Science, Proc. 12th Int. Conf. on Cold Fusion*, A. Takahashi, Y. Iwamura, K. Ota (eds.), World Scientific, Singapore, 2006, pp.44–54.
[3] V.A. Kirkinskii, A.I. Kumelnikov, *Proc. ICCF13*, Sochi, Publisher Center MATI, Moscow, 2007, ISBN 978-5-93271-428-7, pp.43–46.
[4] J.P. Biberian, N. Armanet, ibid. pp.170–180.
[5] T. Nohmi, Y. Sasaki, T. Yamaguchi, A. Taniike, A. Kitamura, A. Takahashi, R. Seto, Y. Fujita, http://www.ler-canr.org; to be published in *Proc. 14th Int. Conf. Condensed Matter Nuclear Science* (ICCF14), Washington, DC, 2008.
[6] G. Alefeld, J. Voelkl (eds.), *Hydrogen in Metals II -Topics in Applied Physics*, Vol. 29, Springer, Berlin, 1978.
[7] A. Koiwai, A. Itoh, T. Hioki, Japan Patent 2005-21860 (P2005-21860A).
[8] C. P. Chang et al., *Int. J. Hydrogen Energy* **16** (1991) 491.
[9] M.M. Antonova, *Sboistva Gidriedov Metallov, Properties of Metal-hydrides*, Naukova Dumka, Kiev, 1975; translated by NissoTsushinsha, Wakayama, 1976 (in Japanese).
[10] Y. Fukai, K. Tanaka, H. Uchida, *Hydrogen and Metals*, Uchida Rokakuho, Tokyo, 1998 (in Japanese).
[11] Y. Sasaki, A. Kitamura, T. Nohmi, Y. Miyoshi, A. Taniike, A. Takahashi, R. Seto, Y. Fujita, *Proc. 9th Meeting of Japan CF-Research Society*, 2009, pp. 29–34; http://www.lenrcanr. org/acrobat/SasakiYdeuteriumg.pdf.
[12] A. Takahashi, A. Kitamura, T. Nohmi, Y. Sasaki, Y. Miyoshi, A. Taniike, R. Seto, Y. Fujita, *Proc. 9th Meeting of Japan CF-Research Society*, 2009, pp. 35–41; http://www.lenrcanr. org/acrobat/TakahashiAdeuteriumg.pdf.
[13] A. Kitamura, T. Nohmi, Y. Sasaki, A. Taniike, A. Takahashi, R. Seto, Y. Fujita, *Phys. Lett.* A, **373** (2009) 3109–3112.
[14] H. Fujita, *J. High Temp. Soc.* **24** (1998) 272.
[15] A. Takahashi, The basics of deuteron cluster dynamics as shown by a Langevin equation, in *LENR Source-Book*, Vol. 2, J. Marwan, S. Krivit (eds.), Washington DC, American Chemical Society, 2009, pp. 193–217.
[16] A. Takahashi, *J. Condensed Matter Nucl. Sci.* **2** (2009) 33–44.